

# We are IntechOpen, the world's leading publisher of Open Access books Built by scientists, for scientists

6,900

Open access books available

186,000

International authors and editors

200M

Downloads

Our authors are among the

154

Countries delivered to

TOP 1%

most cited scientists

12.2%

Contributors from top 500 universities



WEB OF SCIENCE™

Selection of our books indexed in the Book Citation Index  
in Web of Science™ Core Collection (BKCI)

Interested in publishing with us?  
Contact [book.department@intechopen.com](mailto:book.department@intechopen.com)

Numbers displayed above are based on latest data collected.  
For more information visit [www.intechopen.com](http://www.intechopen.com)



---

# Effect of Volcano-Polluted Seawater on the Corrosion Behaviour of Different Alloys

---

Rita Sánchez-Tovar, Ramón Fernández-Domene,  
Rafael Leiva-García, Clara Escrivà-Cerdán,  
Bianca Lucas-Granados and José García-Antón

Additional information is available at the end of the chapter

<http://dx.doi.org/10.5772/63523>

---

## Abstract

During a subsea volcano eruption, gases and thermal water emissions are released. This might change the behaviour of the materials that are in contact with the seawater caused by the decrease of the pH value. For this reason, the materials for marine applications are selected to maintain the integrity of the structure and to be corrosion resistant. In spite of this, corrosion can cause great damage to marine steel infrastructures such as bridges, wharfs, platforms and pipeline systems. These corrosion problems could be aggravated if the medium is altered, due to volcano emissions, since the resistance of the surface film is influenced by the environmental conditions.

Electrochemical techniques are useful to evaluate the corrosion behaviour of different metals and alloys. However, literature regarding the influence of underwater-volcano-polluted seawater on the passivation/corrosion behaviour of stainless steels is scarce. According to this, the objective of the chapter is the evaluation of the influence of an underwater volcano eruption on the corrosion behaviour of different materials that might be used in seawater environments. Electrochemical techniques are applied to evaluate the performance of the different materials when they are immersed in polluted volcano seawater. The results are relevant in the evaluation of natural hazard risk assessments involving critical infrastructures.

**Keywords:** submarine volcano, corrosion, water chemistry, electrochemistry, stainless steels

## 1. Introduction

The aim of natural hazard risk assessment is the evaluation of the extent and nature of risk in a particular area by evaluating potential hazards that together could harm people, property and services. Therefore, an effective natural hazard risk assessment requires the characterisation of both hazards and vulnerabilities of exposed elements [1]. Disasters such as the Eyjafjallajökull eruption in Iceland (2010), or the Tōhoku earthquake and tsunami in Japan (2011), suggest the need for effective natural hazard risk management and sustainable development.

Threats and issues with volcanoes are important, around 600 million people are living in areas that could be affected by volcano eruptions [2]. Therefore, the assessment of the volcano impacts on the different areas together with volcanic monitoring can help to prevent and minimise losses associated with these natural disasters [3]. Among the issues related with volcanoes that can be assessed the effects on critical infrastructures are important. Critical infrastructure is defined as a network of man-made systems and processes that function collaboratively to produce and distribute essential goods and services [4] which are heavily relied upon by society for daily function. Critical infrastructures include electrical supply networks, water and wastewater distribution systems or terrestrial transportation systems. Changes in the chemistry of water sources in the area, tephra falls, lars and lava flows are some of the volcano hazards that can affect to the critical infrastructures. One of the hazards that can affect the critical infrastructures in both short and long term is the corrosion of structural materials.

According to the American Society for Testing and Materials, corrosion can be defined as 'The chemical or electrochemical reaction between a material, usually a metal, and its environment that produces a deterioration of the material and its properties [5]'. Corrosion has serious economical, technological and safety consequences to society. From the economical point of view, it has to be taken into consideration all the costs related with over dimensioning during the design, inspection, maintenance and replacement of the equipment. Several studies performed in different countries have tried to determine the cost of corrosion [6, 7]. The most throughout of these studies was the one conducted in the United States in 1976 which found that the overall annual cost of metallic corrosion to the U.S. economy was \$70 billion, or 4.2% of the gross national product [8]. Besides, any loss of mechanical properties in the metallic materials may lead to an accident with human or environmental consequences. Therefore, any risk-based inspection methodology has to consider the effect of corrosion on infrastructures, and if facilities are installed in areas with volcanic activity, the hazard effects of volcanoes have to be taken into account.

Corrosion is a well-established phenomenon in volcanically active areas [9, 10]. Hydrogen sulphide, gas, SO<sub>2</sub>, CO<sub>2</sub> and other pollutants such as selenium, mercury and arsenic react with oxygen and the atmospheric moisture to produce volcanic smog and acid rain. Thus, those changes in the environment related with volcano eruptions can accelerate the corrosion of the surrounding infrastructures [11]. Specifically, widely distributed volcanic ash derived from explosive volcanic eruption creates short- and long-term hazards to infrastructures including exposed building materials such as metal roofing [12, 13]. The metal corrosion related with

volcanoes has been attributed to volcanic ashes in several studies [14]. In order to study the effect of volcanoes on corrosion, Hawthorn et al. [10] installed a corrosion test site at the Kilauea volcano in Volcanoes National park of the island of Hawaii in 2006. They monitored during 1 year the atmospheric conditions, rainwater chemistry and chlorides deposition. They also exposed some aluminium coupons to the volcano environment. After 1 year of experiments, they observed that the corrosion rate was seven times higher in the volcanic environment than in an industrial site in Oahu [10]. Oze and collaborators also checked the effect of the volcanic ashes on the corrosion of metal roof materials [15]. Increased corrosion of metal roofing from chemically reactive volcanic ash following ash deposition post eruption is a major concern due to the decreasing on the functionality and stability of roofs. They tried to obtain some quantitative information about corrosion rates by coating different materials with volcanic ashes; they could not observe clear trends in the corrosion rates with the performed experiments; however, they observed that in field situations, the corrosion was increased by the presence of volcanic ashes. Therefore, they concluded that volcanic corrosion could be a major problem and the experiments performed had to be improved in order to have into account all the circumstances that can be found in volcanic environments [15]. Therefore, the corrosion induced by the presence of volcanic activity is a problem that has to be taken into consideration during the natural hazards assessments.

However, not too much data have been published on the effect of subaquatic volcanoes on the corrosion of offshore structural materials [16, 17]. Subaquatic volcanoes are normal features on certain regions of the ocean floor. Some may be currently active and, in shallow water, show their actions by blasting steam and debris over the surface of the sea. Many others form at great depths where the weight of the water above them results in confining pressure preventing the violent release of steam and gases. They are estimated to account for 75% of annual magma output. The majority are located near areas of tectonic plate movement (ocean ridges). Submarine volcanoes inject large amounts of material of variable size, texture and chemical composition into the oceans [18]. The state of a submarine eruption evolves from ongoing magmatic activity to highly evolved hydrothermal systems. Some of the features observed during submarine volcanic eruptions are as follows: lava flows, bubbles of lava, lava debris, ash, pumice, steam-blast eruptions, hydrothermal vents, plumes of fine materials and dissolved gas, explosions and discolouration of seawater to light blue and reddish brown. Subaerial volcanos are well characterised; however, there is a lack of study of those in submarine settling [19, 20]. Direct observations of submarine eruptions have been scarce, as they normally occur in remote locations. The first registered underwater eruption was that of the NW Rota in the Southwest Pacific Ocean [21] in 2006. More recently, the dynamic of the Monowai underwater volcano has been described [22]. In all the cases, the carbonate system is modified and the pH reduced as a consequence of the emission of magmatic gas and other compounds [23].

Santiana-Casiano et al. [24] studied the eruption of the island of El Hierro (Canary Islands, Spain) in 2011. This was the first submarine eruption to be monitored from the initial unrest. The eruption started in October 11, 2011, first evidence of eruption was observed in the form of a discolouration of the surface water in the area, going from light green to pale blue to a

brown colour [24]. Those changes may be related to the discharge of high-temperature hydrothermal fluids as well as gases and volcanic particles [25]. Bubbling took place, and the presence of rock fragments was observed floating on the surface of the ocean during the initial steps of the eruption. During the strongest episodes of the eruption, an elevated quantity of dissolved inorganic carbon and a large decrease in the pH value of the surrounding water were observed. The lowest values of pH were concentrated in a layer of 75–100 m of depth; however, due to the intensity of the ejected gases, low values of pH reached the surface water. They also observed at some point during the eruption that the water chemistry of the entire southeast of the island was affected by the presence of the volcano. In April 2012, when the eruption stopped, the system evolved to a hydrothermal system and the pH of the area got to normal values and only some peaks of pH were observed around the area of the volcano [24]. Regarding the dissolved CO<sub>2</sub>, the concentration in the southeast of the island reached levels of 11,000–19,000  $\mu\text{atm}$ , which was an important change in the chemistry of the water. The same rise was observed for sulphur species and oxidants. Therefore, in the event of the eruption of a submarine volcano and the subsequent hydrothermal activity, a change in the chemistry and properties of the seawater in the area should be expected (presence of CO<sub>2</sub>, H<sub>2</sub>S, SO<sub>2</sub>, Fe<sup>2+</sup> and drop in the local pH). Not only submarine eruptions can change the local chemical-physical properties of the water but also passive emissions of gasses and acidic compounds to the environment in islands with volcanic activity can modify the water chemistry. Oceans are a significant store of CO<sub>2</sub>. They exchange it with the atmosphere and provide a reservoir for CO<sub>2</sub>. Therefore, the emissions of CO<sub>2</sub> and other gasses to the environment due to the volcanic activity can decrease the local pH in harbours of volcanic islands.

Those changes can strongly affect the corrosion activity of seawater, raising the probability of corrosion of the metallic materials of the shore and offshore facilities. This corrosion could be generalised, in the case of non-passive materials or localised (pit formation) in the case of passive materials (stainless steels). Corrosion can cause great damage to marine steel infrastructures such as bridges, wharfs, platforms, ships and pipeline systems [26]. These corrosion problems will be aggravated due to the alteration on the chemistry of the water as a consequence of the volcano emissions [27]. Therefore, an adequate selection of the materials and a proper hazard assessment of the volcano effects are very important to predict how some of the critical infrastructures will be affected. Austenitic stainless steel grades 1.4401 (AISI 316) and its derivatives are suitable for shore and offshore service, splash zone applications and temporary immersion in seawater. Duplex stainless steels (e.g. 1.4462/ASTM S31803) may be used in estuaries where the chloride content of the water is lower than that of the open sea. Additionally, superduplex stainless steels (e.g. 1.4410/ASTM S32750) may also be used in direct and continuous contact with seawater (e.g. in offshore oil platforms or desalination plants).

There are some studies dealing with the passivation/corrosion processes of stainless steels in natural seawater [28, 29]. Corrosion studies can be performed in different ways; there are direct measurements (weight loss) and indirect measurements (electrochemical techniques). Electrochemical techniques are useful to evaluate the corrosion behaviour of different metals and alloys in a short period of time providing useful information about the corrosion mechanisms taking place.

According to this, the objective of this chapter will be to evaluate the influence of an underwater volcano eruption on the corrosion behaviour of different materials that might be used in seawater environments. In this way, the electrochemical behaviour of different stainless steels, that is AISI 316 SS and duplex SS, when immersed in solutions which have been polluted by volcano-seawater (collected from the volcano that erupted in the Atlantic Ocean near the island of El Hierro) have been studied. To achieve this objective, different electrochemical techniques have been used, notably open-circuit potential (OCP) measurements, polarization tests and electrochemical impedance spectroscopy (EIS). All these techniques would make possible to achieve a comprehensive view of the corrosion behaviour of stainless steels in volcano seawater. These results may provide and insight in the corrosion effects of volcanic eruptions that could be used in the preparation of natural hazard risk assessments related with volcanoes. This approach has been presented for submarine volcanoes, but the same methodology could be applied to the assessment of corrosion risks due to subaerial volcanoes. In this book chapter, a whole section describing in detail the electrochemical techniques used in the characterisation of the studied stainless steels, has been included, so the readership could better understand the obtained results. These results are used to demonstrate, using electrochemical techniques, that volcano eruptions can negatively affect the lifetime of very important metallic infrastructures, such as harbours, and to establish a link between electrochemistry of materials and volcanology.

## 2. Electrochemical techniques

Since corrosion occurs via electrochemical reactions, electrochemical techniques are useful for the study of the corrosion processes. In these electrochemical techniques, a metal sample is used to model the metal in a corroding environment. The metal sample is immersed in a solution similar to the corroding environment of the metal that is being studied. Additional electrodes are introduced to the system to make an electrochemical cell, which allows measuring the different parameters to study the system. In order to evaluate the effect of volcano-polluted seawater on the corrosion behaviour of different alloys, several electrochemical techniques have been used and they are explained in this section. These techniques are open-circuit potential (OCP), polarization tests and electrochemical impedance spectroscopy (EIS).

### 2.1. Open-Circuit Potential (OCP)

The open-circuit potential (OCP) or corrosion potential is a parameter that indicates the thermodynamically tendency of a material to the electrochemical oxidation in a corrosive medium. According to the ASTM G-15 Standard [5], the OCP is the measured potential between the working electrode and the reference electrode at which there is no current in the circuit. In order to measure the OCP value of a metal, the studied material must be immersed in the solution and after a certain period it stabilizes around a stationary value. When the metal is immersed in the solution, the corrosion starts to occur and electrochemical reactions characteristic of the metal-solution interface take place at the surface of the metal (oxidation

formation of a passive layer or immunity), which can produce variations of the OCP value during the stabilization [5, 30, 31].

## 2.2. Polarization tests

Polarization tests of a metal-electrolyte solution are used in order to characterize the metal by its current-potential relationship. Experimentally, the polarization tests involve changing the potential of the working electrode and register the current as a function of the potential obtaining potentiodynamic curves. Since the current density (the current divided into the area) can experiment high variations, the potentiodynamic curves represent the logarithm of the current density vs the potential [32]. The potential starts at a value lower than the corrosion potential (cathodic region) and increases in the anodic direction. In order to study the repassivation behaviour of a material, the direction of the cyclic potentiodynamic curve can be changed backward to cathodic potentials after achieving a certain current value (once the pitting potential was reached). **Figure 1** shows as an example, a cyclic potentiodynamic curve, with the corresponding corrosion parameters that can be obtained from the curve.

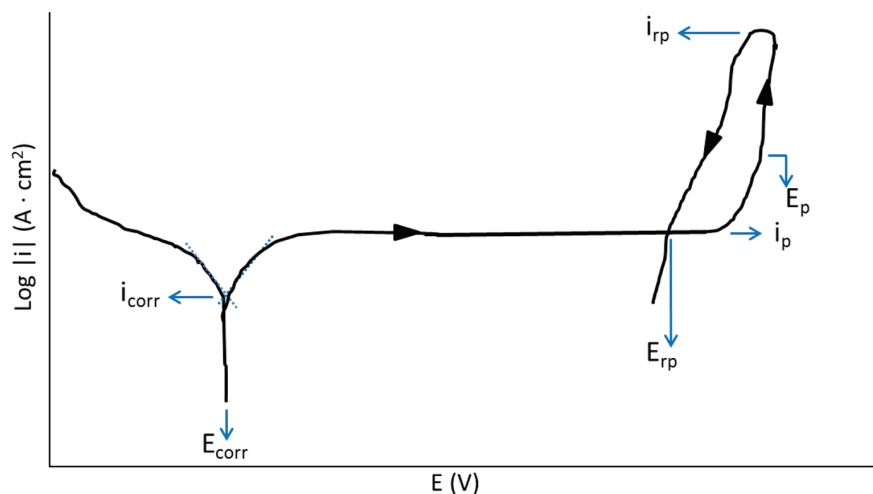


**Figure 1.** Cyclic potentiodynamic curve with the corrosion parameters.  $i_{corr}$ : corrosion current density,  $E_{corr}$ : corrosion potential,  $i_p$ : current density of passivation,  $E_p$ : pitting potential,  $i_{rp}$ : repassivation current density,  $E_{rp}$ : repassivation potential.

When the metal is immersed in the corrosive medium, reduction and oxidation processes occur in its surface. Generally, the metal oxidizes (corrodes) and the medium is reduced both anodic and cathodic currents occur in its surface. If the anodic and cathodic currents are equals in magnitude (i.e. the rate of oxidation and reduction are the same), there is no net current to be measured. The potential at which the current is non-measurable is called corrosion potential ( $E_{corr}$ ).

At potentials more negative than the corrosion potential ( $E < E_{corr}$ ), the cathodic current predominates whereas the anodic current is insignificant, so the curve is in the cathodic region. In contrast, if the potential is more positive than the corrosion potential ( $E > E_{corr}$ ), the predominant current is the anodic one and the curve is in the anodic region [32, 33].

In order to calculate the current density ( $i$ ), the Butler-Volmer equation [Eq. (1)] can be useful as it considers the corrosion of a system with cathodic and anodic reaction.

$$i = i_{corr} \cdot \left[ \exp\left(\frac{2.303 \cdot (E - E_{corr})}{b_a}\right) - \exp\left(-\frac{2.303 \cdot (E - E_{corr})}{b_c}\right) \right] \quad (1)$$

In Eq. (1),  $i$  is the external current density,  $i_{corr}$  is the corrosion current density,  $E$  is the applied potential to polarize the system,  $E_{corr}$  is the corrosion potential,  $b_a$  is the anodic Tafel slope and  $b_c$  is the cathodic Tafel slope. If the applied potential is equal to the corrosion potential then,  $i = i_{corr}$  but if  $E$  is different from  $E_{corr}$  Eq. (1) gives the Tafel law [Eq. (2)]:

$$E = a \pm b \cdot \log |i| \quad (2)$$

where  $a$  is a constant and  $b$  is  $b_a$  or  $b_c$  according to the region of the curve (anodic or cathodic, respectively) [32–34].

In the potentiodynamic curves, for applied potentials more positive than the ones of the cathodic region, in the materials that can be passivated, there is a region where the current density becomes constant (passivation current density,  $i_p$ ). This region is called passivation region, and it is characterized because a passive layer (metal oxide) is formed on the surface of the metal and its chemical reactivity is reduced.

As the applied potential continues increasing, the current density could experiment an abrupt increase and the passive layer could locally breaks by pitting corrosion if the medium contains aggressive ions. The potential at which the pitting corrosion starts is called pitting potential ( $E_{pp}$  when the current density reaches  $100 \mu\text{A}/\text{cm}^2$ ). Finally, if the potential scan is reversed, the current density decreases and eventually the backward curve intersects the forward one: this final region is called repassivation region because the metal recovers the passive state (the potential and current density of the repassivation regions are  $E_{rp}$  and  $i_{rp}$  respectively).

### 2.3. Electrochemical impedance spectroscopy

Electrochemical impedance spectroscopy is a non-destructive technique that is used to study the metal/electrolyte interface. It consists of applying an electrical disturbance (potential) to an electrical circuit in a range of frequencies and measure the current response of the system to each frequency. The applied disturbance of potential can be expressed as a sinusoidal signal as Eq. (3) shows.

$$E = E_0 \cdot \sin(\omega \cdot t) \quad (3)$$

where  $\omega$  is the angular frequency ( $2\pi$  times the conventional frequency in Hz). On the other hand, the current response can also be expressed as a sinusoidal signal that is desphased certain angle ( $\phi$ ), as Eq. (4) shows.

$$I = I_0 \cdot \sin(\omega \cdot t + \phi) \quad (4)$$

The impedance is the quotient of the applied potential and the measured current and it follows the Ohm law; therefore, it can be expressed as Eq. (5) shows.

$$Z = \frac{E}{I} = \frac{E_0 \cdot \sin(\omega \cdot t)}{I_0 \cdot \sin(\omega \cdot t + \phi)} = Z_0 \cdot \frac{\sin(\omega \cdot t)}{\sin(\omega \cdot t + \phi)} \quad (5)$$

where  $Z$  is the complex impedance (which in some electrochemical systems depends on applied potential frequency). The complex impedance can be expressed in terms of a real ( $Z'$ ) and an imaginary component ( $jZ''$ ) as Eq. (6) shows.

$$Z(\omega) = Z_{\text{Re}} - jZ_{\text{Im}} \equiv Z' - jZ'' \quad (6)$$

Plotting the results of the impedances in a correct frequency range, it is possible to extract conclusions about the physical and chemical properties of the materials and the electrochemical systems. Two diagrams are typically extracted from the EIS measurements: Nyquist and Bode diagrams. In the Nyquist diagrams, the real and imaginary components of the impedance at different frequencies are represented. The Bode diagrams represent the  $\log |Z|$  vs  $\log f$  (Bode-modulus), and  $\phi$  vs  $\log f$  (Bode-phase). **Figure 2** shows an example of a Nyquist diagram with the equivalent circuit and an example of a Bode diagram [35, 36].

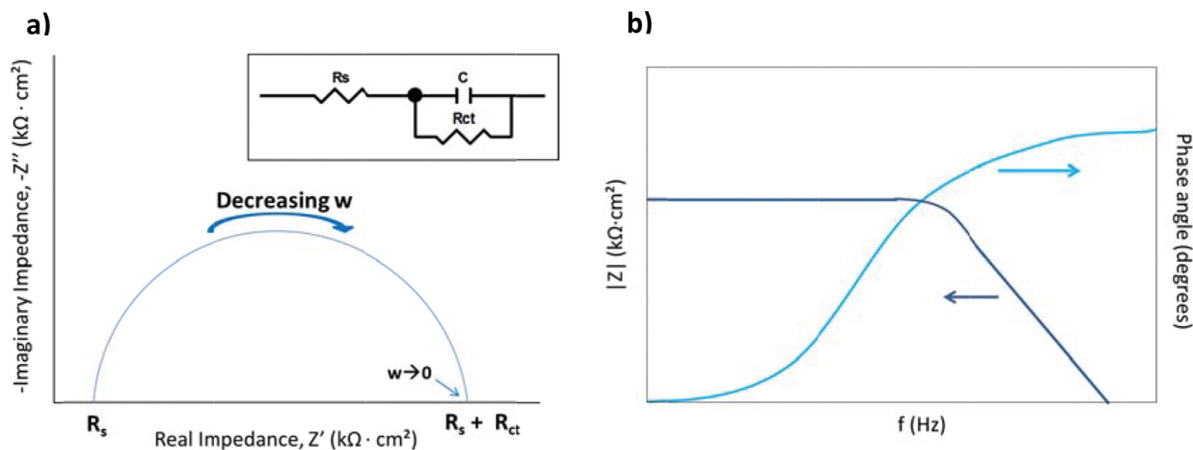


**Figure 2.** Nyquist diagram with the equivalent circuit (a) and Bode-modulus and Bode-phase plots (b).  $R_s$  is the solution resistance and  $R_{ct}$  the charge transfer resistance.

In order to solve the mathematical difficulties in the data treatment of the EIS, the results can be adjusted to an equivalent electrical circuit (**Figure 2**). These circuits try to represent the electrical characteristics of the model and are composed by basic elements such as resistances, capacitances and inductances.

### 3. Experimental procedure

In order to evaluate the influence of an underwater volcano eruption on the corrosion behaviour of different materials, a practical example is detailed in this chapter. In this way, the electrochemical behaviour of different stainless steels, that is AISI 316 stainless steel (SS) and duplex SS, immersed in volcano-seawater (collected from a volcano that erupted in the Atlantic Ocean near the island of El Hierro, Canary Islands, Spain) have been studied. To achieve this objective, different electrochemical techniques have been used. That is OCP measurements, polarization tests and electrochemical impedance spectroscopy (EIS). All these techniques would make possible to achieve a comprehensive view of the corrosion behaviour of stainless steels in volcano seawater.

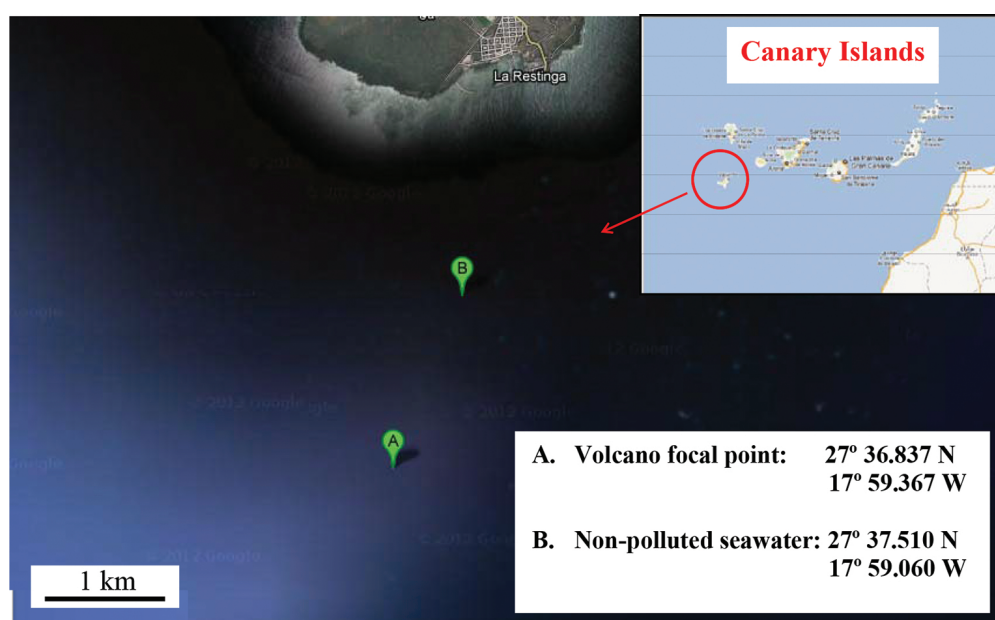


**Figure 3.** Map showing the zones near the island of El Hierro where the non-polluted and polluted seawater samples were taken.

#### 3.1. Materials, solution and electrochemical cell

Experiments were performed in non-polluted (NPS) and polluted seawater (PS). **Figure 3** shows the coordinates where the seawater samples were taken on December 19, 2011. The polluted water was obtained on the focus of the volcano. The non-polluted samples were taken at enough distance to avoid the influence of the pollutants spread by the volcano, following the suggestions of the Spanish National Geographic Institute. Additionally, **Table 1** presents the main parameters of the non-polluted and polluted by the “El Hierro” volcano eruption seawaters. Prior to each experiment the pH and conductivity of the non-polluted and polluted seawater was measured. As shown in **Table 1**, the most substantial difference between both seawaters is pH.

Value	Unpolluted seawater	Polluted seawater
pH	8.02	6.23
Conductivity ( $\mu\text{S cm}^{-1}$ )	65,850	66,400
Sodium ( $\text{mg l}^{-1}$ )	11,080	11,868
Potassium ( $\text{mg l}^{-1}$ )	438	447
Calcium ( $\text{mg l}^{-1}$ )	558	400
Magnesium ( $\text{mg l}^{-1}$ )	1486	1320
Sulphates ( $\text{mg l}^{-1}$ )	2400	2600
Chlorides ( $\text{mg l}^{-1}$ )	20,926	21,200
Bicarbonates ( $\text{mg l}^{-1}$ )	159	220
Carbonates ( $\text{mg l}^{-1}$ )	5.53	0.00

**Table 1.** Composition of both non-polluted and polluted seawater samples, given by the Spanish Institute of Geodesy.

The composition in weight percent of the AISI 316 SS and duplex SS (Alloy 900) used in this work is presented in **Table 2**. The shape of the electrodes was cylindrical, and they have a diameter of 8 mm and a length of 5 mm. They were coated in polytetrafluoroethylene, having an exposed area to the solution of  $0.5 \text{ cm}^2$ . The samples were wet abraded with different silicon carbide papers (from 500 to 4000), and they were finally cleaned with ethanol, distilled water and dried in air.

	Cr	Ni	Mn	Mo	S	Si	P	C	Fe	Cu	N	Ti
AISI 316	16.96	10.17	1.34	2.30	0.00	0.37	0.03	0.08	Bal.	–	–	–
Alloy 900	22.34	4.85	1.59	2.69	–	0.35	0.02	0.03	67.80	0.13	0.20	0.01

**Table 2.** Chemical composition in weight % of AISI 316 and Alloy 900 stainless steels.

An electrochemical vertical cell made of glass was used to carry out the tests. A configuration of three electrodes was used to perform the electrochemical measurements, that is the stainless steel was the working electrode, a platinum wire was the counter electrode and a silver/silver chloride ( $\text{Ag/AgCl } 3\text{M KCl}$ ) was used as reference electrode. All these electrodes were connected to a potentiostat (Autolab PGSTAT302N). The electrochemical tests were repeated at least three times to verify reproducibility of the data obtained in the non-polluted and polluted seawater. The tests were carried out at  $25^\circ\text{C}$ .

### 3.2. OCP measurement and polarization tests

Before each polarization measurement, the open-circuit potential (OCP) was measured for 1 h in the test solution. The average value of the potentials recorded during the last 300 s was the value of the OCP. Afterwards, the potential was shifted to  $-0.25 \text{ V}_{\text{Ag/AgCl}}$  with respect to the OCP, in order to start the polarization measurements. Then, the potential was scanned in the

anodic direction until a value of current density of 10 mA/cm<sup>2</sup> was obtained. In this moment, the potential scan was reversed. The scan rate used to perform the polarization measurements was 0.5 mV s<sup>-1</sup>.

### 3.3. EIS and capacitance measurements

EIS measurements were performed after forming a stable passive film on the surface of the samples at a constant applied potential (-0.1 V<sub>Ag/AgCl</sub>) for 1 h. EIS measurements were conducted at that formation potential in the frequency range of 100 kHz–10 mHz, with a signal amplitude of 10 mV.

## 4. Results and discussion

### 4.1. OCP

The OCP value was calculated as the mean value of the last 5 min of the complete OCP register, which lasted 1 h. The OCP values obtained for the SSs in the different media (polluted and non-polluted seawater) are shown in **Table 3**. In relation to **Table 3**, it can be pointed out that there is no significant influence of the composition of the seawater on the OCP values. On the other hand, the OCP values obtained for Alloy 900 in the non-polluted and polluted seawaters are slightly more negative than those determined for the AISI 316 SS.

Seawater	AISI 316	Alloy 900
Non-polluted	-90 ± 7	-161 ± 2
Polluted	-116 ± 4	-155 ± 8

**Table 3.** Open-circuit potential values for AISI 316 SS and Alloy 900 in both non-polluted and polluted seawater.

### 4.2. Polarization tests

One of the reproducible cyclic polarization curves obtained for the SS in non-polluted and polluted seawater are presented in **Figure 4**. From the polarization curves shown in **Figure 4**, several corrosion and repassivation parameters can be calculated. These parameters, all presented in **Table 4**, are the corrosion potential ( $E_{corr}$ ), the corrosion current density ( $i_{corr}$ ), the passivation current density ( $i_p$ ), pitting potential ( $E_p$ ) and the repassivation potential ( $E_{rp}$ ). The magnitude order of the corrosion potential is the same regardless of the studied media; however, there is an important influence of the seawater on the passivation current densities, which were obtained when the current was stable within the passivation range. Corrosion resistance of these stainless steels is directly associated with a passive film mainly formed by chromium III oxide [37]. It is important to point out that **Table 4** only shows the  $i_p$  values as a measure of the corrosion rates of passive alloys (this parameter has been selected to quantify the corrosion rate instead of  $i_{corr}$  since the SSs used in this work are passivable in the studied media). In relation to the passivation current densities, they importantly increase in polluted

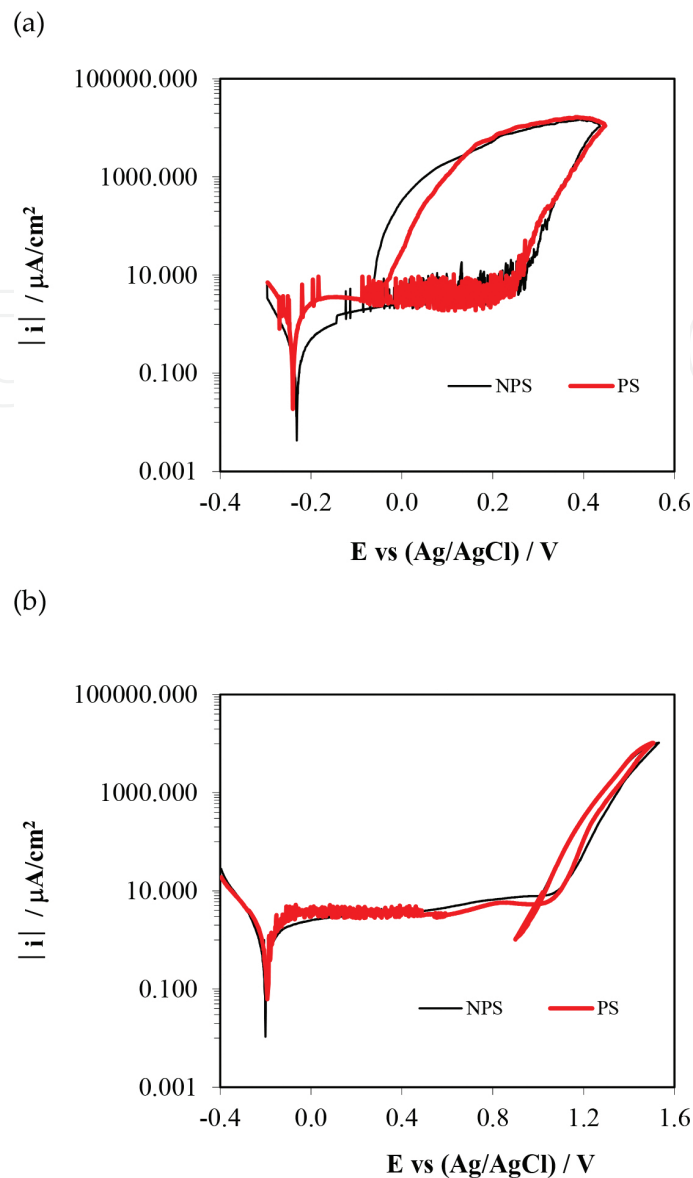


**Figure 4.** Potentiodynamic polarization cyclic curves for AISI 316 SS (a) and Alloy 900 (b) in both non-polluted (NPS) and polluted seawater (PS) solutions at 25°C.

seawater. This fact could be associated to the lower pH which presented this kind of medium. Besides, Alloy 900 SS has higher  $i_p$  values in comparison with the ones obtained for the AISI 316 SS. However, several oscillations in the current density register of the AISI 316 SS in both seawaters and in the register of the Alloy 900 in polluted seawater can be clearly observed in **Figure 4**. These current oscillations indicate that polluted seawater increase the susceptibility of the stainless steels to metastable pitting [38]. In order to evaluate the susceptibility to pitting corrosion of the SS the pitting potential value was evaluated. This parameter is the potential at which the current density reaches  $100 \mu\text{A cm}^{-2}$  and refers to the susceptibility to local breakdown and stable pit initiation [39]. The stainless steels are susceptible to pitting corrosion in both media since chlorides (present in the seawater) are very aggressive ions which are

responsible for the breakdown of the passive films formed on these SSs [39, 40]. **Table 4** shows that the  $E_p$  values for the Alloy 900 are more positive in comparison to AISI 316. This is due to the fact that Duplex SSs, such as Alloy 900, possess a very high resistance to localized corrosion due to their high nitrogen, chromium and molybdenum contents (see **Table 2**). On the other hand, **Table 4** also shows that the values of the pitting potential are similar despite the studied media, but they are to some extent more positive in the non-polluted seawater.

	$E_{corr}$ vs (Ag/AgCl)/mV	$i_p/\mu\text{A cm}^{-2}$	$E_p$ vs (Ag/AgCl)/mV	$E_{rp}$ vs (Ag/AgCl)/mV
Seawater	AISI 316			
Non-polluted	$-230 \pm 8$	$3.89 \pm 0.32$	$309 \pm 10$	$-69 \pm 11$
Polluted	$-239 \pm 5$	$4.66 \pm 0.11$	$302 \pm 7$	$-55 \pm 15$
	Alloy 900			
Non-polluted	$-203 \pm 11$	$4.35 \pm 0.44$	$1220 \pm 47$	$990 \pm 22$
Polluted	$-197 \pm 6$	$5.02 \pm 0.09$	$1200 \pm 29$	$990 \pm 30$

**Table 4.** Electrochemical parameters for AISI 316 SS and Alloy 900 in both non-polluted and polluted seawater, obtained from cyclic polarization curves.

The repassivation potentials were obtained at the crossing point between the backward and forward scans of the polarization curves. This parameter refers to the limit below which the material remains passive and active pits can repassivate. According to this, an  $E_{rp}$  value which is more negative than the corresponding  $E_{corr}$  indicates that the SS is not able to repassivate the pits. Contrary to this, an  $E_{rp}$  value which is more positive than the corrosion potential indicates that the SSs can regenerate an eventual breakdown of the passive film. **Table 4** shows that the repassivation potentials for the studied SS are, in all the studied media, more positive than the corresponding corrosion potential; therefore, the SSs can repassivate the pits.

### 4.3. EIS measurements at an applied anodic potential

In order to characterise the electrochemical behaviour of the passive film/electrolyte interface for the two stainless steels under study, EIS measurements were performed at an applied potential of  $-0.1 \text{ V}_{\text{Ag/AgCl}}$  in both non-polluted and polluted seawater, after a passive film was formed on the electrodes' surface at the same potential. **Figure 5** shows the EIS spectra of AISI 316 and Alloy 900 in the form of Nyquist and Bode plots. In all cases, EIS diagrams exhibit a typical passive state shape characterized by a semicircular shape and high impedance values in Nyquist plots, and by phase angle values close to  $90^\circ$  in Bode-phase plots, suggesting that a stable passive film is formed on all the electrodes [41, 42]. In general, higher impedance values are observed for passive films formed in non-polluted seawater (NPS). The highest impedances are obtained for the duplex stainless steel.

The equivalent electric circuit used to interpret EIS spectra of anodically formed passive films is shown in **Figure 6**. In this equivalent circuit,  $R_s$  represents the electrolyte resistance,  $CPE_1$  is

related to the capacitance of the passive film/electrolyte interface,  $R_1$  corresponds to the charge transfer resistance at that interface and  $Z_{WS}$  is a Warburg impedance, which has been used to interpret the transport of vacancies within the passive film, in the frame of the Point Defect Model [42–44]. The Warburg impedance used here models dimensional diffusion through a layer of finite thickness with absorbing boundary condition [45, 46]:

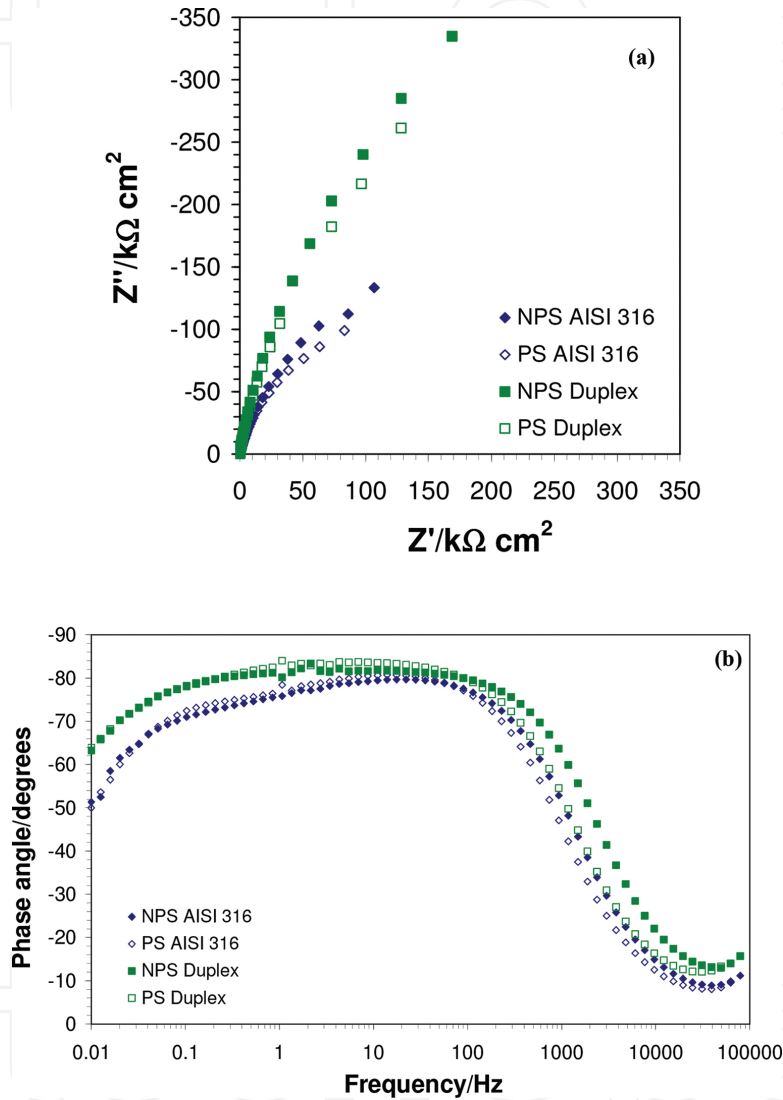


**Figure 5.** Nyquist (a) and Bode-phase (b) plots for AISI 316 and Alloy 900 in both non-polluted (NPS) and polluted seawater (PS) at 25°C, at a film formation potential of  $-0.1\text{ V}_{\text{Ag}/\text{AgCl}}$ .

$$Z_{WS} = \frac{R_W \tanh(B\sqrt{j\omega})}{B\sqrt{j\omega}} \quad (7)$$

where  $B = \delta/(D)^{1/2}$ ,  $\delta$  is the diffusion layer thickness,  $D$  is the diffusion coefficient of the diffusing species,  $R_W$  is the Warburg resistance,  $\omega$  is the angular frequency, and  $j$  is the imaginary unit.

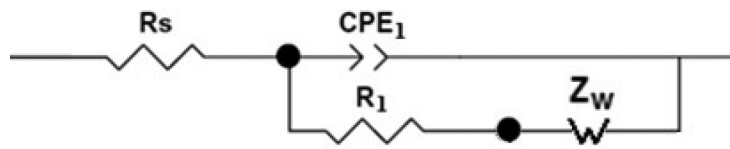


**Figure 6.** Equivalent circuit used to interpret the EIS data.

A constant-phase element (CPE) representing a shift from the ideal capacitor has been used instead of the capacitance itself. The impedance of a constant-phase element is defined as:

$$Q = Z_{CPE} = [C(j\omega)^n]^{-1} \quad (8)$$

where  $n$ , defined as a CPE power, is an adjustable parameter that lies between  $-1$  and  $1$ . For  $n = 1$  the CPE describes an ideal capacitor, and for  $0.5 < n < 1$  the CPE describes a frequency dispersion of time constants due to local heterogeneities in the dielectric material.

The CPE used in the equivalent electric circuit of **Figure 6** has been converted into a pure capacitance ( $C$ ) through the following equation [47, 48]:

$$C = Q^{1/n} (R_s^{-1} + R_1^{-1})^{(n-1)/n} \quad (9)$$

where  $Q = Z_{CPE}$  [Eq. (9)].

The parameters of the equivalent circuit obtained from the fitting procedure are shown in **Table 5**. The values of  $\chi^2$  are of the order of  $10^{-3}$ , indicating that the fittings are good from a mathematical point of view.

		$R_s/\Omega \text{ cm}^2$	$R_1/\text{k} \Omega \text{ cm}^2$	$C_1/\mu\text{F cm}^{-2}$	$n_1$	$R_w/\text{k} \Omega \text{ cm}^2$	$\chi^2 (\times 10^{-3})$
AISI 316	Non-polluted seawater	$5.4 \pm 0.1$	$26 \pm 4$	$16.2 \pm 1.1$	$0.90 \pm 0.01$	$295 \pm 14$	3.8
	Polluted seawater	$4.8 \pm 0.2$	$26 \pm 3$	$24.8 \pm 1.7$	$0.90 \pm 0.01$	$207 \pm 18$	3.7
Alloy 900	Non-polluted seawater	$4.7 \pm 0.3$	$535 \pm 30$	$12.4 \pm 1.3$	$0.91 \pm 0.01$	$753 \pm 53$	3.0
	Polluted seawater	$4.9 \pm 0.3$	$320 \pm 11$	$18.3 \pm 1.2$	$0.92 \pm 0.01$	$544 \pm 18$	2.7

**Table 5.** Equivalent circuit parameters obtained by fitting the experimental results of EIS, for AISI 316 and Alloy 900 in both non-polluted and polluted seawater, at  $-0.1 \text{ V}_{\text{Ag}/\text{AgCl}}$ .

It can be observed from **Table 5** that the charge transfer resistance at the interface,  $R_1$ , is equal or lower, in general, for passive films formed in the polluted seawater. The Warburg resistance,  $R_w$ , follows the same tendency, decreasing in the polluted electrolyte. These results indicate an enhancement of charge transfer processes at the passive film/electrolyte interface and of point defects transport through the passive film for the samples immersed in the polluted seawater, reflecting the poorer protective properties of passive films formed in this electrolyte.

On the other hand, the capacitance of the passive film/electrolyte interface,  $C_1$ , is higher in the polluted seawater. The interfacial capacitance has a strong influence on electrochemical processes in passive systems. This is due to the fact that its characteristics establish the potential drop at the semiconducting passive film/electrolyte interface [42, 49, 50]. Therefore, an increase in  $C_1$  suggests, along with the decrease observed in  $R_1$  and  $R_w$ , that passive films formed in polluted seawater are less protective. The values of the exponent  $n_1$  (lower than unity in all the cases) support the introduction of CPEs in the equivalent circuit rather than pure capacitors.

Concerning the comparison between the protective properties of passive films formed on the two stainless steels under study,  $R_1$  values are significantly lower in the case of AISI 316 (more than 10 times lower than in Alloy 900), and  $R_w$  is the lowest for this stainless steel, as well. Besides,  $C_1$  values for AISI 316 are the highest, regardless of the type of seawater (Table 5). On the other hand, the highest resistances ( $R_1$  and  $R_w$ ) and the lowest interfacial capacitance values ( $C_1$ ) are obtained for the duplex stainless steel (Alloy 900), denoting that passive films formed on Alloy 900 are the most resistant to corrosion in both seawater media.

## 5. Conclusion

The electrochemical techniques used in this work have been proved to be useful in order to study the corrosion behaviour of stainless steels in volcano polluted seawater. From polarization curves, it has been demonstrated that Alloy 900 is more resistant to pitting corrosion than AISI 316. Moreover, the decrease of the charge transfer resistance,  $R_1$ , and the Warburg resistance,  $R_w$ , along with the increase of the interfacial capacitance,  $C_1$ , indicate worse protective properties of passive films formed in the polluted seawater, especially for AISI 316 SS.

Comparing both stainless steels, it can be concluded that passive films formed on Alloy 900 present better protective properties than those of AISI 316 SS.

## Acknowledgements

We wish to express our gratitude to the Ministerio de Ciencia e Innovación (Project CTQ2009-07518), to Prof. Dr. Aurora Santos López, Dr. Rosario Lunar Hernández and Dr. Jose Arnosó Sampedro (Instituto de Geociencias (CSIC, UCM)), Dr. Carmen López Moreno (Head of the Volcano Monitoring Unit, Spanish National Geographic Institute), Humberto Gutiérrez García (Head of the Civil Protection and Emergency Management Service of the General Directorate of Security and Emergencies of the Canary Islands) and Alejandro Ramos Fernández (Coordinador Multisectorial del Centro Coordinador de Emergencias 1-1-2 del Gobierno de Canarias) for their help in supplying both non-polluted and polluted seawater samples.

## Author details

Rita Sánchez-Tovar<sup>1</sup>, Ramón Fernández-Domene<sup>1</sup>, Rafael Leiva-García<sup>2</sup>, Clara Escrivà-Cerdán<sup>1</sup>, Bianca Lucas-Granados<sup>1</sup> and José García-Antón<sup>1\*</sup>

\*Address all correspondence to: jgarciaa@iqn.upv.es

1 Chemical and Nuclear Engineering Department, Polytechnic University of Valencia, Electrochemical Engineering and Corrosion (IEC), Valencia, Spain

2 School of Materials, University of Manchester, Manchester, UK

## References

- [1] UNISDR 2009. *UNISDR Terminology on Disaster Risk reduction*, United Nations, Geneva, Switzerland (2009).
- [2] M.R. Auken, R.S.J. Sparks, L. Siebert, H.C. Crossweller, J. Ewert. *A statistical analysis of the global volcanic fatalities record*. *Journal of Applied Volcanology* 2013, 2: 1–24. doi: 10.1186/s13617-014-0014-6
- [3] R.S.J. Sparks, W.P. Aspinall, H.S. Crossweller, T.K. Hincks. *Risk and uncertainty assessment of volcanic hazards*. In: J. Rougier, R.S.J. Sparks, L. Hill (Eds). *Risk and uncertainty assessment of for natural hazards*. Cambridge University Press, Cambridge (2013), p. 588.
- [4] S.M. Rinaldi, J.P. Peerenboom, T.K. Kelly. *Identifying understanding and analyzing critical infrastructure interdependencies*. *IEEE Control Systems* 2001, 21: 11–25. doi: 10.1109/37.969131
- [5] ASTM G15-89A, Standard Terminology Relating to Corrosion and Corrosion testing. ASTM, Philadelphia (1990).
- [6] T.P. Hoar. *Report of the Committee on Corrosion and Protection—A Survey of Corrosion Protection in the United Kingdom*. HMSO, London (1971).
- [7] C.G. Okamoto *Report of the Committee on Corrosion and Protection—A Survey of the Cost of Corrosion to Japan*, Japan Society of Corrosion Engineering and Japan Association of Corrosion Control (1977).
- [8] *Research Needs Report Energy Convention Research Task force on Energy Conversion Research*, Am. Society of Mechanical Engineering, New York (1976).
- [9] M. Watanabe, A. Hokazono, T. Handa, T. Ichino, N. Kuwani. *Corrosion of copper and silver plates by volcanic gases*. *Corrosion Science* 2006, 48: 3759–3776. doi: 10.1016/j.corsci.2005.12.009

- [10] G.A. Hawthorn, N. Mullet, R. Srinivasan, L.H. Hihara. *Corrosion testing and atmospheric monitoring in an active volcanic environment*. Proceedings of the 2007 Tri-service conference, US Department of Defence (2007).
- [11] R.J. Blong. *Volcanic hazards: a sourcebook on the effects of eruptions*. Academic Press, North Ryde, NSW (1984). p. 424.
- [12] S. Izumo, H. Sueyoshi, K. Kitamura, Y. Ohzono. *Corrosion of metal in volcanic environments*. *Corrosion Engineering* 1990, 39: 271–281.
- [13] R.J. Blong. *Building damage in Rabaul, Papua, New Guinea*. *Bulletin of Volcanology* 2003, 65: 43–54. doi: 10.1007/s00445-002-0238-x
- [14] J. Becker, R. Smith, D. Johnston, A. Munro. *Effects of the 1995–1996 Ruapehu eruptions on communities in central North Island, New Zealand, and people's perceptions of volcanic hazards after the event*. *Australian Journal of Disaster Trauma Studies* 2001, 1: 23.
- [15] C. Oze, J. Cole, A. Scott, T. Wilson, G. Wilson, S. Gaw, S. Hampton, C. Doyle, Z. Li. *Corrosion of metal roof materials related to volcanic ash interactions*. *Natural Hazards* 2014, 71: 785–802. doi: 10.1007/s11069-013-0943-0
- [16] R.M. Fernández-Domene, R. Sánchez-Tovar, C. Escrivà-Cerdán, R. Leiva-García, J. García-Antón. *Study of passive films formed on AISI 316L stainless steel in non-polluted and underwater-volcano-polluted seawater*. *Corrosion* 2014, 70: 390–401. doi: 10.5006/0934
- [17] R.M. Fernández-Domene, R. Sánchez-Tovar, C. Escrivà-Cerdán, R. Leiva-García, J. García-Antón. *Comparison of the effect of non-polluted and underwater-volcano-polluted seawater on the corrosion resistance of different stainless steels*. *Materials and Corrosion*. 2015, 66: 1279–1289. doi: 10.1002/maco.201408172
- [18] V.M. Mantas, A.J.S.C. Pereira, P.V. Morais. *Plumes of discolored water of volcanic origin and possible implications for algal communities. The case of the Home Reef eruption of 2006 ga, Southwest Pacific Ocean*. *Remote Sensing of Environmental* 2011, 115: 1341–1352.
- [19] J.A. Resing, E.T. Baker, J.E. Lupton, K. Nakamura. *Chemistry of hydrothermal plumes above submarine volcanoes of the Mariana Arc*. *Geochemistry Geophysics Geosystems* 2009, 10: Q02009. doi: 0.1029/2008GC002141
- [20] C.E.J. de Ronde, E.T. Baker, G.J. Massoth, J.E. Lupton, I.C. Wright, R.J. Sparks, S.C. Bannister, M.E. Reyners, S.L. Walker, R.R. Greene, J. Ishibashi, K. Faure, J.A. Resing, G.T. Lebon. *Submarine hydrothermal activity along the mid-Kermadec Arc, New Zealand: large-scale effects on venting*. *Geochemistry Geophysics Geosystems* 2007, 8: Q07007.
- [21] R.W. Embley. *Extensive and diverse submarine volcanism and hydrothermal activity in the NE Lau Basin*. *Eos, Transactions, AGU (Fall Meeting Supplement)* 90, abstr. V51D–1719 (2009).
- [22] A.B. Watts. *Rapid rates of growth and collapse of Monowai submarine volcano in the Kermadec Arc*. *Nature Geoscience* 2012, 5: 510–515. doi: 10.1038/ngeo1473

- [23] H. Guillou, J.C. Carracedo, F. Pérez Torrado, E. Rodríguez Badiol. *K-Ar ages and magnetic stratigraphy of a hotspot-induced, fast grown oceanic island: El Hierro, Canary Islands*. Journal of Volcanology and Geothermal Research 1996, 73: 141–155. doi: 10.1016/0377-0273(96)00021-2
- [24] J.M. Santana-Casiano, M. Gonzalez-Davila, E. Fraile-Nuez, D. de Armas, A.G. Gonzalez, J.F. Dominguez-Yanes, J. Escanez. *The natural ocean acidification and fertilization event caused by the submarine eruption of El Hierro*. Scientific Reports Nature 2013, 3: Article number: 1140. doi: 10.1038/srep01140
- [25] K. Nogami, M. Yoshida, J. Osaka. *Chemical composition of discolored seawater around Satsuma-Iwojima, Kagoshima, Japan*. Bulletin Volcanology Society of Japan 1993, 38: 71–77.
- [26] J. Duan, S. Wu, X. Zhang, G. Huang, M. Du, B. Hou. *Corrosion of carbon steel influenced by anaerobic biofilm in natural seawater*. Electrochimica Acta 2008, 54: 22–28. doi: 10.1016/j.electacta.2008.04.085
- [27] L. Freire, M.J. Carmezim, M.G.S. Ferreira, M.F. Montemor. *The passive behaviour of AISI 316 in alkaline media and the effect of pH: a combined electrochemical and analytical study*. Electrochimica Acta 2010, 55: 6174–6181. doi: 10.1016/j.electacta.2009.10.026.
- [28] A. Al Odwani, M. Al-Tabtabaei, A. Abdel-Nabi. *Performance of high chromium stainless steels and titanium alloys in Arabian Gulf seawater*. Desalination 1998, 120: 73–81. doi: 10.1016/S0011-9164(98)00203-3
- [29] S.A. Al-Fozan, A.U. Malik. *Effect of seawater level on corrosion behavior of different alloys*. Desalination 2008, 228: 61–67. doi: 10.1016/j.desal.2007.08.007
- [30] C.J. Brabec, A. Cravino, D. Meissner, N. Serdar Sariciftci, T. Fromherz, M.T. Rispens, L. Sanchez, J.C. Hummelen. *Origin of the open circuit voltage of plastic solar cells*. Advanced Functional Materials 2001, 11: 374–380. doi: 10.1002/1616-3028(200110)11
- [31] G. Berthomé, B. Malki, B. Baroux. *Pitting transients analysis of stainless steels at the open circuit potential*. Corrosion Science 2006, 48: 2432–2441. doi: 10.1016/j.corsci.2005.09.012.
- [32] X.L. Zhang, Zh.H. Jiang, Zh. P. Yao, Y. Song, Zh. D. Wu. *Effects of scan rate on the potentiodynamic polarization curve obtained to determine the Tafel slopes and corrosion current density*. Corrosion Science 2009, 51: 581–587. doi: 10.1016/j.corsci.2008.12.005.
- [33] E. McCafferty. *Validation of corrosion rates measured by the Tafel extrapolation method*. Corrosion Science 2005, 47: 3202–3215. doi: 10.1016/j.corsci.2005.05.046.
- [34] O.A. Petrii, R.R. Nazmutdinov, M.D. Bronshtein, G.A. Tsirlina. *Life of the Tafel equation: current understanding and prospects for the second century*. Electrochimica Acta 2007, 52: 3493–3504. doi: 10.1016/j.electacta.2006.10.014.

- [35] D.V. Ribeiro, J.C.C. Abrantes. *Application of electrochemical impedance spectroscopy (EIS) to monitor the corrosion of reinforced concrete: a new approach*. Construction and Building Materials 2016, 111: 98–104. doi:10.1016/j.conbuildmat.2016.02.047.
- [36] R.L.C. Naumann. Functional Polymer Films: 2 Volume Set. Chapter 25. *Electrochemical Impedance Spectroscopy (EIS)*. Wiley Online Library, Germany. doi: 10.1002/9783527638482.ch25.
- [37] N.E. Hakiki, S. Boudin, B. Rondot, M. Da Cunha Belo. *The electronic structure of passive films formed on stainless steels*. Corrosion Science 1995, 37:1809–1822. doi: 10.1016/0010-938X(95)00084-W
- [38] R.C. Newman. *Understanding the corrosion of stainless steel*. Corrosion 2001, 57: 1030–1041. doi: 10.5006/1.3281676
- [39] M. Kaneko, H.S. Isaacs. *Pitting of stainless steel in bromide, chloride and bromide/chloride solutions*. Corrosion Science 2000, 42: 67–78. doi: 10.1016/S0010-938X(99)00056-6
- [40] M. Kaneko, H.S. Isaacs. *Effects of molybdenum on the pitting of ferritic- and austenitic-stainless steels in bromide and chloride solutions*. Corrosion Science 2002, 44: 1825–1834. doi: 10.1016/S0010-938X(02)00003-3.
- [41] J. Pan, D. Thierry, C. Leygraf. *Electrochemical impedance spectroscopy study of the passive oxide film on titanium for implant application*. Electrochimica Acta. 1996, 41: 1143–1153. doi: 10.1016/0013-4686(95)00465-3.
- [42] R.M. Fernández-Domene, E. Blasco-Tamarit, D.M. García-García, J. García-Antón. *Passive and transpassive behaviour of alloy 31 in a heavy brine libr solution*. Electrochimica Acta 2013, 95: 1–11. doi: 10.1016/j.electacta.2013.02.024.
- [43] D.D. Macdonald, R.Y. Liang, B.G. Pound. *An electrochemical impedance study of the passive film on single crystal Ni(111) in phosphate solutions*. Journal of Electrochemical Society 1987, 134: 2981–2986. doi: 10.1149/1.2100326
- [44] M. Sánchez, J. Gregori, M.C. Alonso, J.J. García-Jareño, F. Vicente, *Anodic growth of passive layers on steel rebars in an alkaline medium simulating the concrete pores*. Electrochimica Acta 2006, 52: 47–53. doi: 10.1016/j.electacta.2006.03.071.
- [45] J. Bisquert, G. Garcia-Belmonte, F. Fabregat-Santiago, P.R. Bueno. *Theoretical models for ac impedance of finite diffusion layers exhibiting low frequency dispersion*. Journal of Electroanalytical Chemistry 1999, 475: 152–163. doi: 10.1016/S0022-0728(99)00346-0
- [46] Z. Grubac, Z. Petrovic, J. Katic, M. Metikos-Hukovic, R. Babic. *The electrochemical behaviour of nanocrystalline nickel: a comparison with polycrystalline nickel under the same experimental condition*. Journal of Electroanalytical Chemistry 2010, 645: 87–93. doi: 10.1016/j.jelechem.2010.04.018.

- [47] G.J. Brug, A.L.G. van den Eeden, M. Sluyters-Rehbach, J.H. Sluyters. *The analysis of electrode impedances complicated by the presence of a constant phase element*. Journal of Electroanalytical Chemistry 1984, 176: 275–295. doi: 10.1016/S0022-0728(84)80324-1.
- [48] B. Hirschorn, M.E. Orazem, B. Tribollet, V. Vivier, I. Frateur, M. Musiani. *Determination of effective capacitance and film thickness from constant-phase-element parameters*. Electrochimica Acta 2010, 55: 6218–6227. doi: 10.1016/j.electacta.2009.10.065.
- [49] J.O. Bockris, K. Uosaki, H. Kita. *Interfacial electron transfer as a significant step in photo-electrochemical reactions on some semiconductors*. Journal of Applied Physics 1981, 52: 808–810. doi: 10.1063/1.328847
- [50] K. Uosaki, H. Kita. *Effects of the Helmholtz Layer capacitance on the potential distribution at semiconductor/electrolyte interface and the linearity of the Mott-Schottky plot*. Journal of Electrochemical Society 1983, 130: 895–897. doi:10.1149/1.211985

